Synthesis and characterization of carbazolo[2,1-*a*]carbazole in thin film and single crystal field-effect transistors†

Miriam Más-Montoya,[a‡] José Pedro Cerón-Carrasco,[b] Shino Hamao,[c] Ritsuko Eguchi,[c] Yoshihiro Kubozono,[c,*] Alberto Tárraga,[a] and David Curiel.[a,*]

[a.] *Department of Organic Chemistry, Faculty of Chemistry, University of Murcia, Campus of Espinardo, 30100-Murcia, Spain.*
[b.] *Bioinformatics and High Performance Computing Group, Universidad Católica San Antonio de Murcia (UCAM), Avda. Jerónimos, 135, 30107 Guadalupe, Murcia, Spain.*
[c.] *Research Institute for Interdisciplinary Science, Okayama University, Okayama 700-8530, Japan.*
‡Present address: Molecular Materials and Nanosystems, Institute for Complex Molecular Systems, Eindhoven University of Technology, P.O. Box 513, 5600 MB Eindhoven, The Netherlands.
†Electronic Supplementary Information (ESI) available: NMR spectra, TGA and DSC thermograms, and additional OFET characteristics. See DOI: 10.1039/x0xx00000x

The synthesis of a hexacyclic fused polyheteroaromatic system, namely carbazolo[2,1-*a*]carbazole, using a simple two-step route is reported. Additionally, the characterization of its electronic structure is described, corresponding to a very stable molecule that is also transparent to the visible light. The solid state packing is determined by X-ray diffraction analysis which, in combination with the computational calculation of the charge transfer parameters, reveals an adequate molecular arrangement to achieve a low anisotropic environment for charge transport. This π-conjugated system is used as organic semiconductor for the fabrication of thin film and single crystal organic field-effect transistors (OFETs). Furthermore, the evaluation of different gate dielectrics results in transistors with very good hole mobilities and low operating voltages. In agreement with these results, carbazolo[2,1-*a*]carbazole becomes some of the best organic semiconductors belonging to the family of carbazole-based azaphenacenes.

Introduction

Organic semiconductors have emerged as alternative materials to the traditional semiconductors having inorganic nature. The promising technical properties of organic materials which could lead to cheap, light-weight and flexible electronic devices have motivated great interest in research for the development of this technology.[1-5] Nevertheless, certain issues basically related to the typical disorder of molecular solids, which makes more difficult the charge transport, or the degradation of optoelectronic devices due to the sensitivity of the organic semiconductors, still need to be addressed. Accordingly, a plethora of π-conjugated systems have been synthesized to explore the effect of different structural alterations on the charge transport ability of organic materials.[6-8] In this regard, among the group of materials classified as small molecules, fused polyaromatic or polyheteroaromatic structures represent a bench mark for charge transport studies. Linear acenes such as pentacene have been comprehensively studied rendering high charge mobilities.[9, 10] However, the instability of acenes under ambient conditions requires that alternative materials have to be explored.[11] Accordingly, armchaired phenacenes, which have better stability due to their lower HOMO (Highest Occupied Molecular Orbital) energies, have also proved to be excellent organic semiconductors in thin film and single crystal OFETs.[12-16] Closely related to this family of compounds, the replacement of benzene rings by thiophene rings brings on the series of thienoacenes,[17, 18] which have produced some of the best hole mobilities for organic materials.[19] Additionally, if the pyrrole ring is integrated in the fused polyheteroaromatic structure, similar azaphenacene systems can be prepared. Although lower charge mobilities have been reported so far within this latter series of organic semiconductors, the presence of pyrrole rings introduces interesting features, since the reactivity of the nitrogen atom permits the chemical derivatization of the π-conjugated system.[20, 21] This opens infinite possibilities for the tuning of electronic properties and solubility using simple synthetic methodologies. As a result, many studies have been published mainly based on the structure of indolo[3,2-*b*]carbazoles.[22-25] Unfortunately, despite the good results reported for some of them and their potential application in organic electronics, with a few exceptions, the diversity of azaphenacene cores including the pyrrole unit is still quite scarce.[26-30] Therefore, the ample margin for improving the charge transport properties within this group of materials encouraged us to synthesize and study π-extended compounds resulting from the fusion of two carbazole units that constitute the series of carbazolocarbazoles.[31] Herein, we report the utilization of the carbazolo[2,1-*a*]carbazole isomer, **2**, as organic semiconductor. Although this molecule was first described long ago,[32] the lack of convenient synthetic methods might have restricted its applicability.[33] Consequently, we present an

alternative methodology that consists in a regiospecific route of two steps only. Moreover, the electronic structure of carbazolo[2,1-*a*]carbazole shows a low lying HOMO which makes it very stable towards ambient oxidation. Therefore, organic field effect transistors have been fabricated using both thin films and single crystals. Preliminary studies carried out with the plain carbazolo[2,1-*a*]carbazole system have rendered thin film OFETs which significantly improve the results previously reported for other carbazolocarbazole isomers and are certainly comparable to more sophisticated indolocarbazole derivatives. What is more important, single crystal OFETs, which become ideal devices for the study of organic semiconductors with few defects and high purity,[34-36] have displayed excellent characteristic parameters placing carbazolo[2,1-*a*]carbazole among the best carbazole-based azaphenacenes with still a promising room for improvement.

Results and discussion

Synthesis and characterization.

Compound **2** was synthesized as depicted in Scheme 1. Initially, a double *N*-arylation based on a Buchwald-Hartwig reaction between 1,5-diaminonaphthalene and *ortho*-dibromobenzene led to the intermediate product, **1**.[37] Subsequently, a photoinduced unimolecular radical nucleophilic substitution, under basic conditions, permitted the isolation of the carbazolo[2,1-*a*]carbazole.[38] The structures of the intermediate and final products were elucidated by the usual spectroscopic techniques (see Experimental Section and Electronic Supplementary Information).

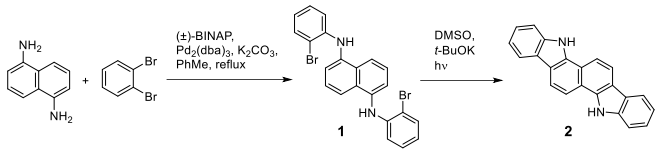

Scheme 1 Synthetic route to carbazolo[2,1-*a*]carbazole, **2**.

Thermal stability is a requirement for any organic material that intervenes in the fabrication of optoelectronic devices. Therefore, the thermal characterization of **2** was carried out by thermogravimetric analysis, which did not display any significant mass loss (5%) up to 380 °C. Additionally, differential scanning calorimetry experiments did not evidence any phase transition during the heating and cooling cycles (Fig. S3, ESI). These results confirm the aptitude of carbazolocarbazole **2** as a thermally stable molecule.

As far as the absorption spectrum of carbazolo[2,1-*a*]carbazole is concerned, it showed a well resolved vibrational structure with several bands ascribed to different π-π^* transitions (Fig. 1). The lower energy band ($\lambda_{max.}$= 380 nm, ε= 2.4×10^4 M^{-1}cm^{-1}) corresponded to a wide HOMO-LUMO (Lowest Unoccupied Molecular Orbital) gap of 3.22 eV, making this compound transparent to the visible radiation. This represents an interesting feature regarding the possibility of developing logic gate circuits or devices where the transparency of semiconducting materials is a required condition.[39, 40] The UV-vis spectrum obtained for a thin film presented the expected bathochromic shift ($\lambda_{max.}$= 390 nm) due to the intermolecular interactions in the solid state.

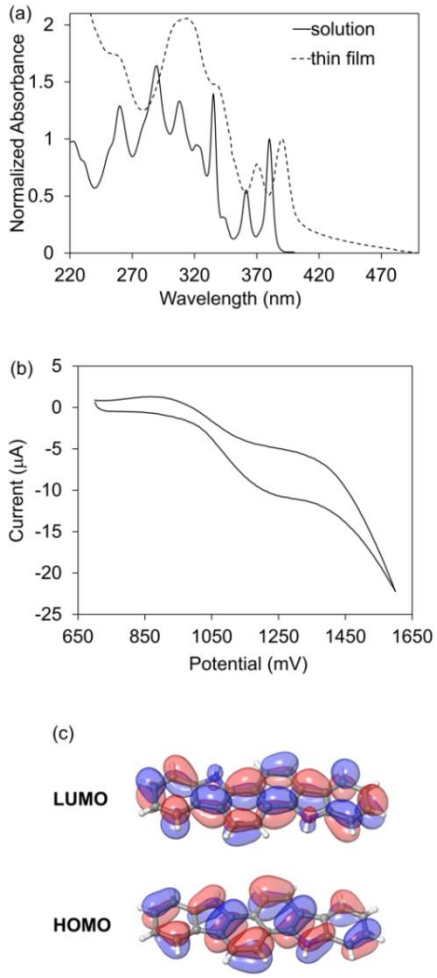

Fig. 1 (a) Absorption spectra (continuous plot: 10^{-5} M THF, T=25°C; dashed plot: thin film); (b) Cyclic voltammetry (10^{-3}M THF, $TBAPF_6$ 0.1 M, Pt working electrode, SCE reference electrode, scan rate: 100 mVs^{-1}, T=25°C); (c) Frontier orbitals calculated isosurfaces (isovalue: 0.20 a.u.).

The electronic structure was completed by determining the oxidation potential from cyclic voltammetry measurements (Fig. 1). An irreversible wave was obtained with an anodic peak potential at 1250 mV. Curiously, despite the benzenoid structure of compound **2**, the irreversibility of the cyclic voltammetry contrasts to the reversible behavior found for other carbazolocarbazole isomers.[31] Anyhow, the onset of the oxidation wave locates at 980 mV and it can be used for calculating a HOMO energy of -5.68 eV, lower than any of the previously reported carbazolocarbazoles. The low lying HOMO confers high stability to this material towards ambient oxidation. Additionally, the LUMO energy (-2.46 eV) was estimated by difference from the optical HOMO-LUMO gap, determined from the onset of the lower energy band in the UV-vis spectrum. Both frontier orbitals are distributed along the entire π-conjugated structure as it is verified by the isosurfaces determined by DFT calculations (Fig. 1).

This extended distribution of the isosurfaces will have a beneficial effect on the intermolecular charge transfer, due to the higher probability of "in phase" molecular orbital overlap that improves the electronic coupling when the molecules are adequately arranged in the solid state.[41, 42] Thus, bearing in mind that charge transport properties in organic semiconductors are critically conditioned by the solid state structure,[43, 44] the molecular packing of carbazolo[2,1-*a*]carbazole was determined by single crystal X-ray diffraction (Fig. 2 and 4). The fused hexacyclic system shows a perfectly flat structure. When the crystalline network is extended according to the van der Waals contacts of an arbitrarily chosen molecule, this is surrounded by six more molecules interacting through face-to-face and edge-to-face interactions which define a herringbone packing. The molecules packed in parallel planes display an interplanar distance of 3.2 Å.

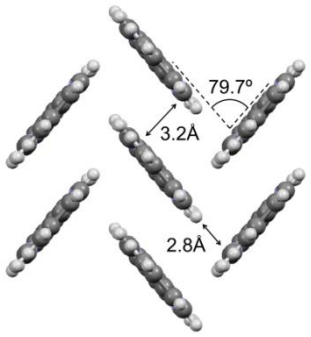

Fig. 2 Herringbone packing of **2** determined by X-ray diffraction.

Thin film transistors.

Thin film OFETs with a top-contact/bottom-gate architecture were prepared by thermal evaporation of compound **2** (60 nm) on silicon substrates (not heated), covered by a layer of SiO_2 (400 nm) or ZrO_2 (150 nm) working as dielectrics. Moreover, a thin film of parylene (30 nm) was previously deposited by thermally assisted polymerization onto the dielectric layer. Parylene functions as a low permittivity insulator whose hydrophobicity and pinhole free surface have proved very useful for improving the electronic and morphological properties at the organic semiconductor/dielectric interfaces.[45] Additionally, due to the low lying HOMO of carbazolo[2,1-*a*]carbazole, contact doping was applied by using a thin layer of F_4TCNQ between the semiconductor and the gold top electrodes. This has been demonstrated to decrease the Schottky barrier at the metal/semiconductor interface favouring charge carrier injection.[46-48] Accordingly, the OFETs fabricated with a SiO_2 dielectric (400 nm thick) were characterized using a two probe mode under inert gas atmosphere (Table 1). These transistors displayed output characteristics with an excellent slope variation along the linear regime, reaching the saturation current at the expected drain voltage for the series of curves measured at gate voltages between 0 V and -80 V (Fig. S4, ESI). Concerning the transfer characteristics, OFETs showed very little hysteresis (Fig. S4, ESI). The best results were obtained for channel dimensions of W=500 µm and L=450 µm, reaching a hole mobility of 0.17 $cm^2\ V^{-1}\ cm^{-1}$, with a threshold voltage of -19 V, $I_{on/off}$=3×10^6 and subthreshold swing, S=7 V dec^{-1}. Optimization of the gate dielectric material can contribute to the increase of charge carrier concentration in the conduction channel at the semiconductor/dielectric interface, which could consequently result in decreasing the operating voltage of the transistor and benefiting the charge mobility.[49, 50] In agreement with this premise, analogous OFETs fabricated with higher-k gate dielectric such as ZrO_2 resulted in a noticeably improved device performance. Lower operating voltages were used, with output characteristics being measured between 0 and -18V (Fig. 3). Besides, no hysteresis was detected in the transfer curves as a consequence of the higher ZrO_2 capacitance and possibly a reduced trap concentration. Among the characteristic parameters, it is worth highlighting the reduction in the threshold voltage (-6.4 V) and the S factor (0.7 $Vdec^{-1}$). Moreover, hole mobility in the saturation regime was 0.24 $cm^2V^{-1}cm^{-1}$ and $I_{on/off}$= 6×10^4.

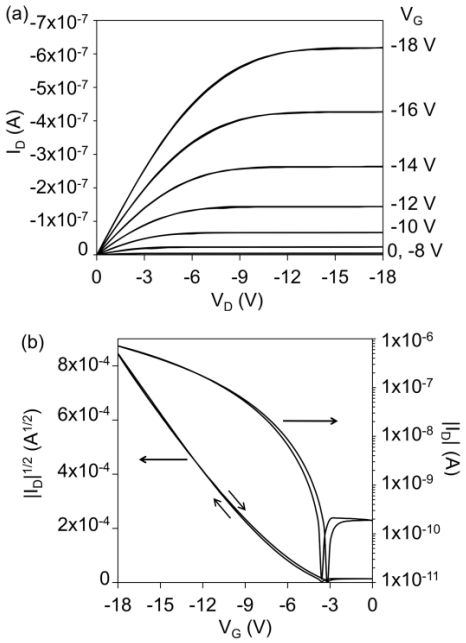

Fig. 3 (a) Output and (b) transfer characteristics for V_D =-18 V of a thin film OFET (Si/ZrO_2/Parylene/**2**/F_4TCNQ/Au).

Table 1 Characteristic parameters of thin film OFETs.

Parameter		Dielectric	
		SiO_2[a]	ZrO_2[b]
μ	best	0.17	0.24
[$cm^2V^{-1}s^{-1}$]	avg. ± σ[c]	0.13 ± 0.04	0.23 ± 0.03
V_T [V]	best	-19	-6.4
	avg. ± σ[c]	-21 ± 3	-6.3 ± 0.1
$I_{on/off}$	best	3×10^6	6×10^4
	avg. ± σ[c]	$(1 \pm 2)\times10^6$	$(2 \pm 3)\times10^4$
S_{factor}	best	7	0.7
[$Vdec^{-1}$]	avg. ± σ[c]	5 ± 1	0.6 ± 0.1

[a] V_D = -80 V; [b] V_D = -18 V; [c] σ= standard deviation.

These results not only get better than those previously reported for other carbazolocarbazole isomers but also emphasize the interest of a structurally simple molecule such as carbazolo[2,1-*a*]carbazole when compared to more intrincate indolocarbazole-based materials.[51, 52] In order to get a better understanding of the good functioning of the carbazolo[2,1-*a*]carbazole OFETs, which should be related to the disposition of the molecules in the thin film, X-ray diffraction analysis was carried out for the thin film evaporated on the SiO_2/Si substrate. The resulting diffractogram was perfectly coincident with the (h00) reflections determined for the single crystal (Fig. 4). Diffraction peaks up to the fourth order were detected, evidencing a highly ordered material in the crystalline films. Thus, it could be assumed that the previously described molecular arrangement is maintained in the semiconductor thin film. In agreement with this result, the carbazolocarbazole molecules tend to adopt an edge-on orientation, standing on the *a** direction with the *bc*-plane of the thin film parallel to the substrate surface.

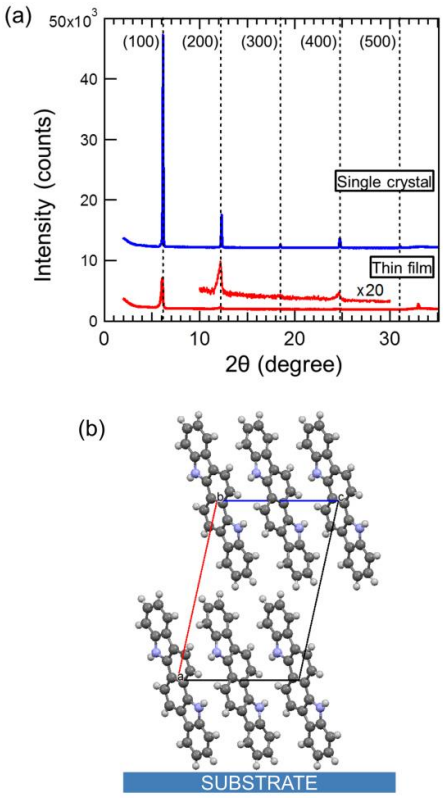

Fig. 4 (a) Single crystal and thin film X-ray diffractograms of **2**; (b) Idealized view along the *b* axis of the molecular of orientation of **2** on the substrate.

Furthermore, computational calculations based on the above described molecular packing enabled the determination of the transfer integral and the reorganization energy of compound **2**. The intermolecular electronic coupling was calculated for two different orientations (Fig. 5). Those molecules packed in parallel planes showed a HOMO transfer integral value ($t_{f\text{-}f}$) of 58 meV. The face-to-face interactions between stacked molecules denote a HOMO overlap as depicted in the computational studies performed for the dimer (Fig. 6). In the case of molecules whose packing is governed by edge-to-face interactions the HOMO transfer integral ($t_{e\text{-}f}$) is 60 meV.

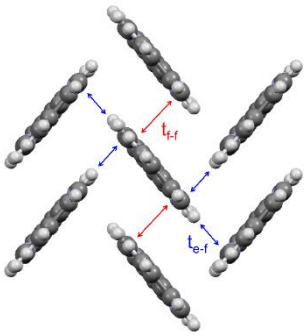

Fig. 5 Calculated transfer integrals for the solid-state structure of **2** ($t_{f\text{-}f}$=58 meV; $t_{e\text{-}f}$=60 meV).

The similarity between these electronic parameters results in a favourable low anisotropic environment for the charge transport along the length of channel of the transistor. Consequently, this correlates well with the measured hole mobilities. Moreover, the satisfactory bidirectional transfer integrals compensate the moderate reorganization energy calculated for the compound **2** (λ_h=194 meV).

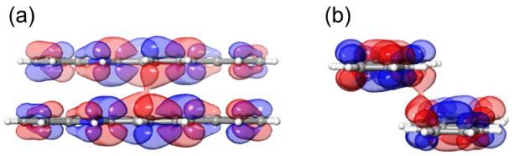

Fig. 6 Calculated HOMO isosurfaces of the carbazolo[2,1-*a*]carbazole face-to-face stacked dimer ((a) view along the short axis; (b) view along the long axis).

Single crystal transistors.

Since single crystal OFETs generally show charge transport properties which overcome the typical limitations of thin films due to the higher purity and more ordered solid state structure, single crystals of **2** were grown by gradient sublimation using argon as the gas carrier. The FET properties were fully investigated in top-contact/bottom-gate devices. Bearing in mind the previously discussed benefit of high-k dielectrics, different materials were also studied for the single crystal OFETs. With the aim of being rigorous on these initial studies with **2**, we not only kept the same device architecture but we also used the same sequence of materials. In this regard, the semiconducting crystal was placed onto a layer of parylene that had been previously deposited on the dielectric. Subsequently, a thin film of F_4TCNQ and the gold electrodes were sequentially evaporated to complete the contacts. As expected for the single crystal OFETs, devices fabricated with SiO_2 (300 nm) dielectric showed a remarkable increase in the hole mobility, reaching a maximum value of 0.8 $cm^2\ V^{-1}\ cm^{-1}$ (Table 2). Other parameters which also improved when compared to thin film transistors were the threshold voltage (-12 V) and the subthreshold swing (1.8 V dec^{-1}). Conversely, a decrease in the intensity on/off ratio was measured. It is worth mentioning at this point that despite the presence of F_4TCNQ interfacial layer, all the fabricated single crystal OFETs showed certain contact resistance as evidenced by the curvature at the origin of the output characteristics (Fig. S5, ESI).

When higher-k material such as ZrO_2 (150 nm) was employed as gate dielectric, a noticeable reduction in the operating voltage was observed. This was also accompanied by a favourable decrease in the subthreshold swing. Accordingly, quite low threshold voltage (-4 V) was measured, along with a *S*-factor = 0.6 $Vdec^{-1}$. The hole mobility determined from the transfer curves was 0.4 $cm^2V^{-1}s^{-1}$ (Fig. S6, ESI). Interestingly, in contrast to the overall enhancement observed for the characteristic parameters when comparing the single crystal transistors based on SiO_2 dielectric to the corresponding thin film devices, such a difference is not that significant for devices fabricated with ZrO_2 dielectrics which reinforces the adequacy of this material to be further explored in OFETs. Additionally, when the ceramic perovskite $PbZr_{0.52}Ti_{0.48}O_3$ (PZT) (150 nm) was used as dielectric in single crystal OFETs fabricated with **2**, the device performance was further improved (Fig. 7).

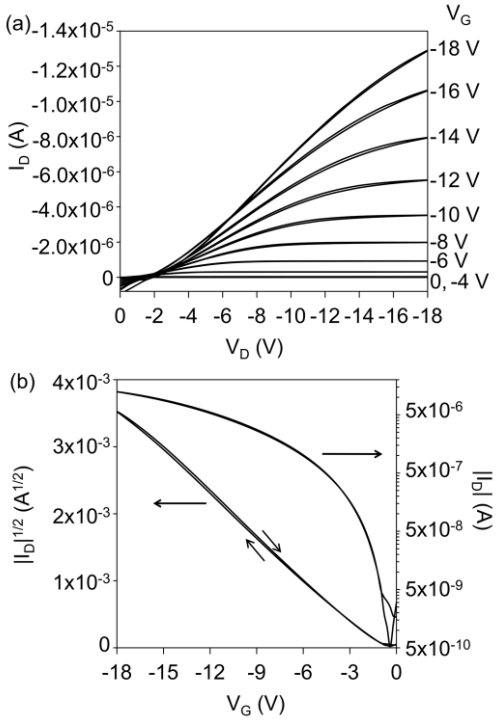

Fig. 7 (a) Output and (b) transfer characteristics for V_D = -18 V of a single crystal OFET (Si/PZT/Parylene/**2**/F_4TCNQ/Au).

The hole mobility reached a best value of 1 $cm^2V^{-1}s^{-1}$. More importantly, the threshold voltage was reduced to -2 V with a subthreshold swing as low as 0.8 $Vdec^{-1}$. A beneficial effect on the $I_{on/off}$ ratio was also detected (2×10^4) when compared to the transistors fabricated with SiO_2 or ZrO_2 dielectrics. Besides, virtually no hysteresis was detected in the transfer characteristics. Considering that the contact resistance should still be optimised, this leaves room for improving the performance of the above described single crystal OFETs.

Anyhow, these results correspond, to the best of our knowledge, to one of the best OFETs reported up until now for carbazole-based azaphenacenes, proving the potential of carbazolo[2,1-*a*]carbazole as organic semiconductor.

Table 2 Characteristic parameters of single crystal OFETs.

Parameter		Dielectric		
		SiO_2[a]	ZrO_2[b]	PZT[c]
μ	best	0.8	0.4	1.0
[$cm^2V^{-1}s^{-1}$]	avg.± σ[d]	0.7±0.1	0.3±0.1	0.9±0.1
V_T [V]	best	-12	-4	-2
	avg.± σ[d]	-32±18	-5±2	-2.1±0.3
$I_{on/off}$	best	2×10^3	6×10^3	2×10^4
	avg.± σ[d]	$(3\pm3)\times10^4$	$(4\pm3)\times10^3$	$(2.5\pm0.2)\times10^4$
S_{factor} [$Vdec^{-1}$]	best	1.8	0.6	0.8
	avg.± σ[d]	2.6±0.7	0.7±0.1	0.6±0.3

[a] V_D = -80 V; [b] V_D = -16 V; [c] V_D = -18 V; [d] σ= standard deviation.

Experimental

General. Reagents used as starting materials were purchased from commercial sources and were used without further purification. Solvents were dried following the usual protocols (Toluene was distilled from sodium wire with benzophenone indicator). Unless stated otherwise, all reactions were carried out under nitrogen atmosphere. Column chromatography was run with silica gel 60 A CC 70-200 µm as stationary phase, using HPLC grade solvents. Melting points were measured in a Reichert instrument and are not corrected. Unless stated otherwise, all spectra were recorded at room temperature. ^{1}H-NMR and ^{13}C-NMR spectra were recorded on a Bruker AV400 or a Bruker AV600 spectrometers having frequencies of 400MHz or 600MHz, for proton nuclei and 100 MHz, or 150MHz, respectively, for carbon nuclei. Chemical shifts are referred to the residual peak from the deuterated solvent. Mass spectrometry was recorded on HPLC-MS TOF 6220 instrument. Absorption spectra were recorded on a Cary 5000 UV-vis-NIR spectrophotometer. Electrochemistry was recorded utilizing a Bass potenciostate and using platinum electrodes as working and

counter-electrode and SCE as reference electrode. Thermogravimetric analysis was carried out at a heating rate of 10 °Cmin^{-1} under nitrogen.

***N,N'*-bis(2-bromophenyl)naphthalene-1,5-diamine, 1:** A stirred suspension of (±)-BINAP (0.12 g, 0.19 mmol) in dry toluene (10 mL) under nitrogen atmosphere was heated at 80 °C until BINAP was completely dissolved. Then, a solution of $Pd_2(dba)_3$ (0.12 g, 0.13 mmol) in dry toluene (5 mL) was added and the mixture was stirred at room temperature for 15 minutes. The resulting solution was added via syringe to a mixture of 1,5-diaminonaphthalene (0.4 g, 2.53 mmol), 1,2-dibromobenzene (1.31 g, 5.55 mmol), and K_2CO_3 (2.1 g, 15.2 mmol) in dry toluene (20 mL) under nitrogen atmosphere. The reaction mixture was refluxed for 5 days. After cooling, the crude was washed with brine and dried over anhydrous Na_2SO_4. The solvent was removed under reduced pressure and the residue was purified by column chromatography on silica gel using dichloromethane:hexane (1:2) as eluent to obtain **1** as a pure solid (0.3 g, 25 %). M.p.: 157 °C. ^{1}H NMR (400 MHz, $CDCl_3$, ppm): δ 7.91 - 7.83 (m, 2H), 7.57 (dd, *J* = 8.0, 1.4 Hz, 2H), 7.50 - 7.42 (m, 4H), 7.15 - 7.06 (m, 2H), 6.90 (dd, *J* = 8.2, 1.5 Hz, 2H), 6.73 (ddd, *J* = 8.0, 7.3, 1.5 Hz, 2H), 6.42 (s, 2H, NH). ^{13}C NMR (100 MHz, $CDCl_3$, ppm): δ 142.9, 137.9, 132.8, 130.4, 128.2, 126.2, 120.4, 119.8, 118.9, 115.6, 111.4. HRMS (ESI-TOF) *m/z*: $[M+H]^+$ Calcd for $C_{22}H_{17}Br_2N_2$ 466.9753, found: 466.9741.

Carbazolo[2,1-*a*]carbazole, 2: Anhydrous DMSO (230 mL) was deoxygenated in a photochemical reactor for 15 minutes. Then, *t*-BuOK (0.60 g, 5.3 mmol) was added and the mixture was further deoxygenated for 10 minutes. Subsequently, **1** (0.62 g, 1.32 mmol) was added and the reaction mixture was irradiated with a mercury vapour lamp for 90 minutes. After cooling, the crude was quenched with a saturated solution of ammonium chloride. The resulting precipitate was filtered over a celite pad and redissolved in THF. Next, the solvent was evaporated under reduced pressure and the solid residue was treated with methanol to precipitate the desired compound (0.31 g, 76 %). The isolated solid was further purified by gradient sublimation under high vacuum conditions. M.p. > 300 °C. ^{1}H NMR (600 MHz, DMSO, ppm): δ 12.17 (s, 2H, NH), 8.33 (d, *J* = 8.5 Hz, 2H), 8.25 (d, *J* = 8.5 Hz, 2H), 8.19 (d, *J* = 7.8 Hz, 2H), 7.64 (d, *J* = 8.0 Hz, 2H), 7.41 (t, *J* = 7.5 Hz, 2H), 7.23 (t, *J* = 7.4 Hz, 2H). ^{13}C NMR (150 MHz, DMSO, ppm): δ 138.8, 136.2, 124.4, 123.3, 119.6, 119.1, 119.0, 118.7, 117.2, 113.1, 111.2. HRMS (ESI-TOF) *m/z*: $[M+H]^+$ Calcd for $C_{22}H_{13}N_2$ 305.1073, found: 305.1075.

X-ray Structure Determination: The single crystal X-ray data were collected at 100 K with a Bruker D8Quest Kappa Diffractometer using CuKα radiation. The structure was solved using direct methods and refined on F2 by full-matrix least-squares method, using SHELX-2013 software package and expanded using Fourier techniques. All non-hydrogen atoms were refined anisotropically. Hydrogen atoms were found by Fourier difference map and were treated as a riding model except to N1H01 that was refined as free with Dfix.

The out-of-plane XRD patterns of thin film and single crystal of **2** (Fig. 4a) were measured using a Smart Lab-Pro (Rigaku) with an X-ray wavelength of 1.5418 Å (CuKα source).

Computational details. The geometry of **2** was fully optimized at the B3LYP/6-311G(d,p) level of theory as neutral and cationic forms. Single-point calculations were subsequently conducted to determine the hole reorganization energy (λ_h) by using:

$$\lambda_h = \left[E_M^+ - E_{M^+}^+\right] + \left[E_{M^+} - E_M\right]$$

where E_M and E_M^+ stand for the energy of the neutral and the cation in the optimized neutral geometry, while E_{M^+} and $E_{M^+}^+$ are the energies of the neutral and cation in the optimized cation structure, respectively. The crystal structure was next used to determine the electronic coupling (t_{ab}) between the central monomer and all its surrounding molecules, which measures the efficiency of the charge-transport processes. All quantum calculations were performed with the Jaguar program as implemented in the Schrödinger Material Science Suite.

OFETs fabrication and Characterization. Compound **2** was purified by gradient sublimation at 10^{-6} Torr prior to OFET fabrication. 60 nm-thick thin films of **2** were fabricated on gate dielectrics (SiO_2 and ZrO_2) formed on Si substrates by thermal deposition below 10^{-7} Torr. Surfaces of the gate dielectrics were modified by single-layer of HMDS for SiO_2 and coated with 50 nm-thick parylene for ZrO_2 in the formation of thin films. The above substrate was maintained at room temperature during thermal deposition. On the other hand, single crystals of **2** were placed on various gate dielectrics (SiO_2, ZrO_2 and PZT). Surfaces of gate dielectrics were coated with 50 nm-thick parylene in placing the single crystals. Single crystals were prepared using physical vapor transport method in which high-temperature zone for putting the powder sample and low-temperature zone for collecting single crystals were 380 and 180 °C, respectively; Ar gas was flowed at 50 mLmin^{-1}. Details of single crystal preparation are described elsewhere.[12-16] 50 nm-thick gold (Au) source/drain electrodes were formed on the thin film or single crystal of **2** by thermal deposition below 10^{-7} Torr. A 3 nm-thick layer of 2,3,5,6-tetrafluoro-7,7,8,8-tetracyanoquinodimethane (F_4TCNQ) was inserted between Au electrodes and the thin film or single crystal to reduce the contact resistance. The FET properties were measured in two-terminal measurement mode using a semiconductor parameter analyzer (Agilent B1500A). The capacitance per area, C_o's, for the gate dielectrics at 0 Hz were measured using a precision LCR meter (Agilent E4980A); the C_o values were 8.3 nF cm^{-2} for 400 nm-thick SiO_2 (HMDS-treated), 9.5 nF cm^{-2} for 300 nm-thick SiO_2 (50 nm-thick parylene-coated), 40 nF cm^{-2} for ZrO_2 (50 nm-thick parylene-coated) and 40 nF cm^{-2} for PZT (50 nm-thick parylene-coated).

Conclusions

In summary, a simple two-step synthetic route has been described for the preparation of carbazolo[2,1-*a*]carbazole. The characterization of this azaphenacene by thermal methods, absorption spectroscopy and cyclic voltammetry, has evidenced a high

thermal stability, as well as a wide optical gap with a low lying HOMO, that confers transparency to the visible light and high stability towards ambient oxidation respectively. Additionally, single crystal X-ray diffraction revealed a herringbone packing. This solid state arrangement was further confirmed to persist in thin films. Based on the crystal packing, charge transfer parameters such as transfer integral and reorganization energy were calculated by computational methods. The transfer integrals revealed that an advantageous environment with a little anisotropy in the charge transfer parameters was present in the carbazolo[2,1-*a*]carbazole solid state structure. This favours the charge transport by this azaphenacene as it was evidenced by the characterization of field-effect transistors. Thin film transistors, where interfacial engineering was performed both at the metal contacts and at the semiconductor/dielectric interface, displayed very good performance. Considering that these devices were prepared using not heated substrates, the achieved hole mobility (0.24 $cm^2V^{-1}s^{-1}$) and threshold voltage (-6.4 V) place the carbazolo[2,1-*a*]carbazole OFETs as some of the best devices reported so far for carbazole-based azaphenacenes, even when compared to molecules with a more complicated structure. Finally, the evaluation of different high-k gate dielectrics for the fabrication of single crystal OFETs, reached excellent characteristic parameters with hole mobilities as high as 1 $cm^2V^{-1}s^{-1}$ and threshold voltages as low as -2 V. Therefore, it can be concluded that these preliminary results obtained for the core structure of carbazolo[2,1-*a*]carbazole make it into a promising semiconductor with still a wide margin to be further improved and explored in the area of organic electronics.

Acknowledgements

Authors gratefully acknowledge the Spanish Ministry of Economy and Competitivity (Project: CTQ2014-58875-R) for the financial support.

Notes and references

1 R.-P. Xu, Y.-Q. Li and J.-X. Tang, *J. Mater. Chem. C*, 2016, **4**, 9116-9142.
2 B. Kang, W. H. Lee and K. Cho, *ACS Appl. Mater. Interfaces*, 2013, **5**, 2302-2315.
3 H. T. Yi, M. M. Payne, J. E. Anthony and V. Podzorov, *Nat. Commun.*, 2012, **3**, 1259.
4 F. C. Krebs, *Sol. Energy Mater. Sol. Cells*, 2009, **93**, 394-412.
5 M. Pagliaro, R. Ciriminna and G. Palmisano, *ChemSusChem*, 2008, **1**, 880-891.
6 J. Mei, Y. Diao, A. L. Appleton, L. Fang and Z. Bao, *J. Am. Chem. Soc.*, 2013, **135**, 6724-6746.
7 C. Wang, H. Dong, W. Hu, Y. Liu and D. Zhu, *Chem. Rev.*, 2011, **112**, 2208-2267.
8 H. Dong, C. Wang and W. Hu, *Chem. Commun.*, 2010, **46**, 5211-5222.
9 O. D. Jurchescu, M. Popinciuc, B. J. van Wees and T. T. M. Palstra, *Adv. Mater.*, 2007, **19**, 688-692.
10 O. D. Jurchescu, J. Baas and T. T. M. Palstra, *Appl. Phys. Lett.*, 2004, **84**, 3061-3063.
11 X. Shi and C. Chi, *Chem. Rec.*, 2016, **16**, 1690-1700.
12 Y. Shimo, T. Mikami, S. Hamao, H. Goto, H. Okamoto, R. Eguchi, S. Gohda, Y. Hayashi and Y. Kubozono, *Sci. Rep.*, 2016, **6**, 21008.
13 H. Okamoto, R. Eguchi, S. Hamao, H. Goto, K. Gotoh, Y. Sakai, M. Izumi, Y. Takaguchi, S. Gohda and Y. Kubozono, *Sci. Rep.*, 2014, **4**, 5330.
14 R. Eguchi, X. He, S. Hamao, H. Goto, H. Okamoto, S. Gohda, K. Sato and Y. Kubozono, *Phys. Chem. Chem. Phys.*, 2013, **15**, 20611-20617.
15 Y. Sugawara, Y. Kaji, K. Ogawa, R. Eguchi, S. Oikawa, H. Gohda, A. Fujiwara and Y. Kubozono, *Appl. Phys. Lett.*, 2011, **98**, 013303/013301-013303/013303.
16 H. Okamoto, N. Kawasaki, Y. Kaji, Y. Kubozono, A. Fujiwara and M. Yamaji, *J. Am. Chem. Soc.*, 2008, **130**, 10470-10471.
17 K. Takimiya, M. Nakano, M. J. Kang, E. Miyazaki and I. Osaka, *Eur. J. Org. Chem.*, 2013, **2013**, 217-227.
18 K. Takimiya, S. Shinamura, I. Osaka and E. Miyazaki, *Adv. Mater.*, 2011, **23**, 4347-4370.
19 H. Minemawari, T. Yamada, H. Matsui, J. y. Tsutsumi, S. Haas, R. Chiba, R. Kumai and T. Hasegawa, *Nature*, 2011, **475**, 364-367.
20 P.-L. T. Boudreault, S. Wakim, N. Blouin, M. Simard, C. Tessier, Y. Tao and M. Leclerc, *J. Am. Chem. Soc.*, 2007, **129**, 9125-9136.
21 Y. Wu, Y. Li, S. Gardner and B. S. Ong, *J. Am. Chem. Soc.*, 2005, **127**, 614-618.
22 I. Cho, S. K. Park, B. Kang, J. W. Chung, J. H. Kim, K. Cho and S. Y. Park, *Adv. Funct. Mater.*, 2016, **26**, 2966-2973.
23 G. Zhao, H. Dong, L. Jiang, H. Zhao, X. Qin and W. Hu, *Appl. Phys. Lett.*, 2012, **101**, 103302.
24 H. Jiang, H. Zhao, K. K. Zhang, X. Chen, C. Kloc and W. Hu, *Adv. Mater.*, 2011, **23**, 5075-5080.
25 Y. Guo, H. Zhao, G. Yu, C.-a. Di, W. Liu, S. Jiang, S. Yan, C. Wang, H. Zhang, X. Sun, X. Tao and Y. Liu, *Adv. Mater.*, 2008, **20**, 4835-4839.
26 K. S. Park, S. M. Salunkhe, I. Lim, C.-G. Cho, S.-H. Han and M. M. Sung, *Adv. Mater.*, 2013, **25**, 3351-3356.
27 J.-Y. Balandier, N. Henry, J.-B. Arlin, L. Sanguinet, V. Lemaur, C. Niebel, B. Chattopadhyay, A. R. Kennedy, P. Leriche, P. Blanchard, J. Cornil and Y. H. Geerts, *Org. Lett.*, 2013, **15**, 302-305.
28 L. Qiu, C. Yu, N. Zhao, W. Chen, Y. Guo, X. Wan, R. Yang and Y. Liu, *Chem. Commun.*, 2012, **48**, 12225-12227.
29 T. V. Pho, J. D. Yuen, J. A. Kurzman, B. G. Smith, M. Miao, W. T. Walker, R. Seshadri and F. Wudl, *J. Am. Chem. Soc.*, 2012, **134**, 18185-18188.
30 M. Sonntag and P. Strohriegl, *Tetrahedron*, 2006, **62**, 8103-8108.
31 M. Mas-Montoya, R. P. Ortiz, D. Curiel, A. Espinosa, M. Allain, A. Facchetti and T. J. Marks, *J. Mater. Chem. C*, 2013, **1**, 1959-1969.
32 M. Zander and W. H. Franke, *Chem. Ber.*, 1969, **102**, 2728-2738.
33 F. Dufour and G. Kirsch, *J. Heterocycl. Chem.*, 2008, **45**, 161-163.
34 L. Jiang, H. Dong and W. Hu, *J. Mater. Chem.*, 2010, **20**, 4994-5007.

35 Z. Bao and J. Locklin, *Organic Field-Effect Transistors*, CRC Press Taylor & Francis Group, Boca Raton, 2007.
36 R. W. I. de Boer, M. E. Gershenson, A. F. Morpurgo and V. Podzorov, *Phys. Status Solidi A*, 2004, **201**, 1302-1331.
37 P. Ruiz-Castillo and S. L. Buchwald, *Chem. Rev.*, 2016, **116**, 12564-12649.
38 M. E. Budén, V. A. Vaillard, S. E. Martin and R. A. Rossi, *J. Org. Chem.*, 2009, **74**, 4490-4498.
39 A. Facchetti and T. J. Marks, *Transparent Electronics: From Synthesis to Applications*, John Wiley & Sons Ltd., 2010.
40 J. F. Wager, D. A. Keszler and R. E. Presley, *Transparent Electronics*, Springer, New York, 2008.
41 V. Coropceanu, H. Li, P. Winget, L. Zhu and J.-L. Brédas, *Annu. Rev. Mater. Res.*, 2013, **43**, 63-87.
42 J. L. Brédas, J. P. Calbert, D. A. da Silva Filho and J. Cornil, *Proc. Natl. Acad. Sci.*, 2002, **99**, 5804-5809.
43 H. Dong, X. Fu, J. Liu, Z. Wang and W. Hu, *Adv. Mater.*, 2013, **25**, 6158-6183.
44 J. A. Lim, H. S. Lee, W. H. Lee and K. Cho, *Adv. Funct. Mater.*, 2009, **19**, 1515-1525.
45 V. Podzorov, V. M. Pudalov and M. E. Gershenson, *Appl. Phys. Lett.*, 2003, **82**, 1739-1741.
46 C. Liu, Y. Xu and Y.-Y. Noh, *Mater. Today*, 2015, **18**, 79-96.
47 T. Minari, T. Miyadera, K. Tsukagoshi, Y. Aoyagi and H. Ito, *Appl. Phys. Lett.*, 2007, **91**, 053508.
48 X. He, S. Hamao, R. Eguchi, H. Goto, Y. Yoshida, G. Saito and Y. Kubozono, *J. Phys. Chem. C*, 2014, **118**, 5284-5293.
49 R. P. Ortiz, A. Facchetti and T. J. Marks, *Chem. Rev.*, 2010, **110**, 205-239.
50 A. Facchetti, M. H. Yoon and T. J. Marks, *Adv. Mater.*, 2005, **17**, 1705-1725.
51 P.-L. T. Boudreault, A. A. Virkar, Z. Bao and M. Leclerc, *Org. Electron.*, 2010, **11**, 1649-1659.
52 P.-L. T. Boudreault, S. Wakim, M. L. Tang, Y. Tao, Z. Bao and M. Leclerc, *J. Mater. Chem.*, 2009, **19**, 2921-2928.